

The effect of Coulomb field on laser-induced ultrafast imaging methods

XiaoLei Hao¹, YuXing Bai¹, XiaoYun Zhao¹, Chan Li¹, JingYu Zhang¹, JiLing Wang¹, WeiDong Li^{1,*},
ChuanLiang Wang^{2,5}, Wei Quan², XiaoJun Liu^{2,†}, Zheng Shu³, Mingqing Liu³, and Jing Chen^{3,4‡}

¹*Institute of Theoretical Physics and Department of Physics,*

State Key Laboratory of Quantum Optics and Quantum Optics Devices,

Collaborative Innovation Center of Extreme Optics, Shanxi University, Taiyuan 030006, China

²*State Key Laboratory of Magnetic Resonance and Atomic and Molecular Physics,*

Wuhan Institute of Physics and Mathematics, Innovation Academy for Precision Measurement Science and Technology,

Chinese Academy of Sciences, Wuhan 430071, China

³*Institute of Applied Physics and Computational Mathematics, P.O. Box 8009, Beijing 100088, China*

⁴*Center for Advanced Material Diagnostic Technology,*

Shenzhen Technology University, Shenzhen 518118, China. and

⁵*Present address: School of Physics and Electrical Engineering, Kashgar University, Kashgar 844006, China*

(Dated: March 17, 2020)

By performing a joint theoretical and experimental investigation on the high-order above-threshold ionization (HATI) spectrum, the dominant role of the 3rd-return-recollision trajectories in the region near the cutoff due to the ionic Coulomb field is identified. This invalidates the key assumption adopted in the conventional laser-induced electron diffraction (LIED) approach that the 1st-return-recollision trajectories dominate the spectrum according to strong field approximation (SFA). Our results show that the incident (return) electron beams produced by the 1st and 3rd returns possess distinct characteristics of beam energy, beam diameter and temporal evolution law due to the influence of Coulomb field, and therefore the extracted results in the LIED will be altered if the significance of the 3rd-return-recollision trajectories is properly considered in the analysis. Such Coulomb field effect should be taken into account in all kinds of laser-induced imaging schemes based on recollision.

PACS numbers: 33.80.Rv

As one of the most important processes in strong field physics, recollision has provided an unprecedented insight into the inner working of atoms and molecules [1, 2]. In recollision picture, one electron is liberated from the target atom or molecule through tunneling ionization and then be accelerated in the field and pulled back by the field to collide with the parent ion. Most intriguing phenomena in strong field physics, such as high-order above-threshold ionization(HATI), high harmonics generation(HHG) and nonsequential double-ionization(NSDI), can be well understood based on the recollision physics (see, e.g., [3–6] for reviews and references therein).

Since the products upon recollision carry information of the parent ion, they can be used to probe the structure of the parent ion. Various methods have been proposed to image molecules in intense laser fields based on the analysis of different products upon recollision, such as laser-induced electron diffraction (LIED) [7–12], molecular clock[13–16], tomographic imaging of orbitals [17, 18] and laser-induced inelastic diffraction (LIID) [19]. Since these methods are self-imaging approaches based on coherent electron scattering, they can provide an unprecedented spatial-temporal resolution. In general, as long as the imaging method is based on electron scattering, the

resolution of extracted results will depend upon the parameters of the incident electron beam, such as the beam energy, the beam diameter and the temporal evolution of the beam. Unlike the conventional electron diffraction (CED) method in which the information of the incident electron beam is well known, the incident (return) electron beam in the self-imaging method is produced by the laser-induced ionization of the target itself and its information is much more complicated. In LIED, for example, the temporal resolution relies on the knowledge of the temporal evolution of the beam, and more specifically, deconvolution of the exact recollision time. In the recollision process, however, the electron may miss the parent ion at the 1st return but collide with it at the subsequent returns as illustrated in Fig. 1 (a), which results in a large uncertainty in the recollision time. To complicate matters further, the incident energy and the impact parameter for different returns vary. In LIED, the aforementioned complexity is largely ignored by applying the strong field approximation (SFA) wherein the Coulomb interaction between the parent ion and the freed electron is ignored. According to SFA, the maximal kinetic energy at collision for 1st-return-recollision trajectories is much higher than that for multiple-return-recollision trajectories. Thus, the high energy part of the photoelectron momentum distribution selected for analysis in LIED is assumed to be produced mostly by the 1st-return-recollision trajectories. Furthermore, due to the spread of the electron wavepacket, the probability of the multiple-return-recollision trajectories is much smaller.

*Electronic address: wdli@sxu.edu.cn

†Electronic address: xjliu@wipm.ac.cn

‡Electronic address: chen.jing@iapcm.ac.cn

Nevertheless, more and more studies have shown that the Coulomb field plays an important role in the ionization dynamics of atoms and molecules in intense laser fields [20–25]. Specially, the Coulomb focusing effect will significantly improve the contribution of the multiple-return-recollision trajectories [26, 27] and in some cases it will even exceed that of the 1st return [15, 28, 29] in inelastic recollision process. Therefore, the basic assumption on the incident electron beam in the ultrafast imaging method may be in question, and, the impact of the Coulomb field on the imaging results has to be carefully accessed. In this paper, we theoretically and experimentally investigate the plateau in ATI spectrum and a distinct laser pulse duration dependence of the plateau is revealed. Analysis shows that this dependence is closely related to the increasing contribution of the 3rd-return-recollision trajectories due to the effect of Coulomb field. For multi-cycle laser field, this contribution becomes even dominant in the near-cutoff HATI spectrum. Since electron beams associated with the 1st and 3rd returns show distinct time evolution characteristic and impact parameter distribution, using the 3rd-return-recollision trajectories for analysis in LIED will change the imaging results.

In Fig. 1 we present the photoelectron energy spectra calculated with classical-trajectory Monte Carlo method (CTMC) (Fig. 1(b)) and numerical solution of time-dependent Schrödinger equation (TDSE) (Fig. 1(c)), and also the measured spectra (Fig. 1(d)), for Ar atoms exposed to intense laser pulses with different pulse durations at peak intensity of $1.25 \times 10^{14} \text{W/cm}^2$ and center wavelength of 800 nm. The details of the CTMC method [23, 30, 31] are presented in the supplementary material. The TDSE is solved using the freely available software QPROP [32]. In both calculations, the hydrogen-like Coulomb potential is applied. The linearly polarized laser field has a sine-square pulse envelope in the form of $E(t) = E_0 \sin^2(1.14t/\tau_p) \cos(\omega t + \varphi_0)$, where φ_0 is the carrier-envelope phase (CEP), τ_p is the duration of the pulse. Here the pulse duration is defined as the full width at half maximum (FWHM) of the intensity. The measured results are obtained with CEP unlocked, and correspondingly, in calculation of CTMC each trajectory is calculated with random CEP, and in TDSE the spectra are averaged over different CEPs with regular interval of $\pi/8$.

In our experiment (see supplementary material for details), the laser beam is introduced into the vacuum chamber of a homemade time-of-flight (TOF) photoelectron kinetic energy spectrometer [33, 34] with a limited detection angle of 0.026 sr (opening angle of 5°) in the direction of laser polarization. To compare directly with the measured spectra in Fig. 1(d), only trajectories with momentum direction in the corresponding range of $\theta_p < 5^\circ$, where θ_p is the angle between the final momentum and the laser polarization, are considered to obtain the CTMC spectra (Fig. 1(b)). For TDSE, in Fig. 1(c) we present the spectra along the direction of the laser polarization, i.e. $(\mathbf{dw}/\mathbf{dEd}\Omega)|_{\theta=\varphi=0}$. The ATI peaks

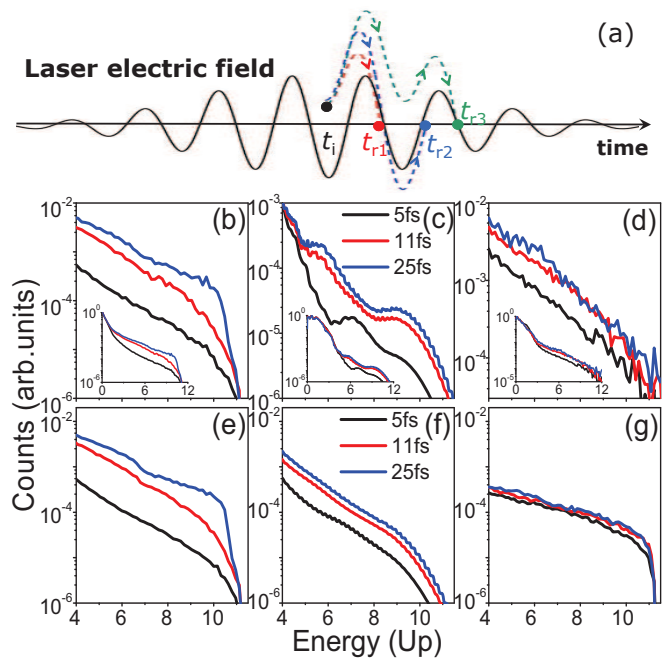


FIG. 1: (Color online) (a) Sketch map to illustrate the multiple-return-recollision trajectories. For a multicycle laser field, after the electron is ionized through tunneling at t_i , it may come back to collide with the core upon the first return at t_{r1} or miss the core and collide with it at t_{r2} , t_{r3} ... (b)-(g) Simulated and measured ATI spectra for Ar atoms exposed to laser pulses with different durations at peak intensity of $1.25 \times 10^{14} \text{W/cm}^2$ and center wavelength of 800 nm. (b)-(d) show CTMC, TDSE and measured high energy part of the spectra in the direction of polarization, respectively. The insets present the entire spectra. (e) and (f) show angle-integrated spectra calculated by CTMC and TDSE, respectively. (g) shows the angle-integrated spectra calculated with CTMC by employing the Yukawa potential in the evolution of electrons, while all other spectra in Fig. 1 are calculated in hydrogen-like Coulomb potential.

in TDSE spectra are smoothed over by averaging adjacent data points to make the variation of the plateau more visible. All spectra in Fig. 1 are normalized to themselves by dividing the maximum of the individual spectrum. The simulated and measured entire spectra (insets in Figs. 1(b)-(d)) exhibit the well-documented ATI spectral features, i.e., a rapid decrease within $2U_p$ followed by a plateau extending to $10U_p$. If we focus on the dependence of the plateau on pulse duration, a qualitative agreement can be found between simulations (Figs. 1(b), (c)) and measurement (Fig. 1(d)). The yield of the plateau first increases quickly when pulse duration increases from 5 fs to 11 fs, then only increases slightly until the pulse duration increases to 25 fs [35]. In Figs. 1(e) and (f), we also present the angle-integrated spectra calculated by CTMC and TDSE to show that the pulse duration dependence is also prominent in the case of high-acceptance-angle with which LIED measurement is performed. This is not surprising, because the ma-

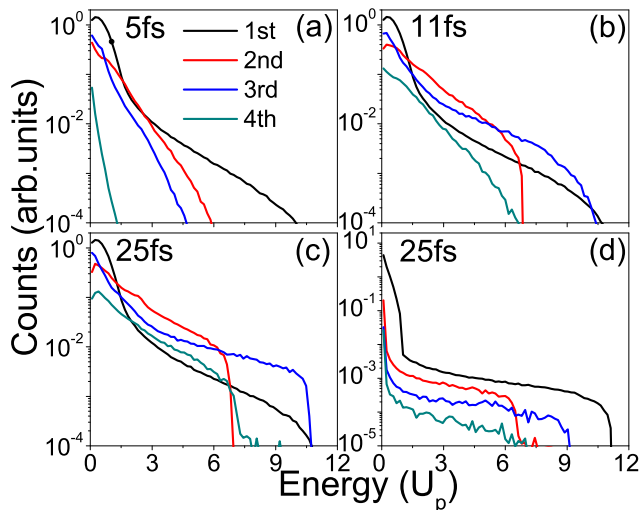


FIG. 2: (Color online) CTMC calculated spectra with angle integrated for different returns of recollision trajectories for Ar atoms in laser pulses at peak intensity of $1.25 \times 10^{14} \text{ W/cm}^2$ and wavelength of 800 nm. (a)-(c) Spectra calculated using hydrogen-like Coulomb potential for different pulse durations as indicated in the figures. (d) Spectra calculated using Yukawa potential for pulse duration of 25 fs.

majority of photoelectrons will move along the polarization direction in linearly polarized laser field.

In the following we try to understand the pulse duration dependence of the plateau with CTMC approach by taking advantage of the transparent intermediate process that can be explored with this approach. If we employ the Yukawa potential instead of the Coulomb potential in the evolution of electrons after leaving the tunnel exit in CTMC, the spectra become independent of the pulse duration as shown in Fig. 1(g). The Yukawa potential is of the form $V(r) = -(Z'/r) \exp(-r/a)$, with parameters $Z' = 4.547$ and $a = 4$ which are chosen to retain the ground-state energy of Ar by TDSE. Therefore, the pulse duration dependence of the plateau comes from the effect of the ionic Coulomb potential.

Next we will show how the Coulomb field affects the plateau of the ATI spectrum. The pulse duration dependence of the plateau in Fig. 1 indicates that some specific multiple-return-recollision trajectories contribute significantly to the plateau. In the CTMC model, the different return recollision trajectories can be distinguished according to the travel time t_t defined as the interval between the ionization time and the recollision time. For trajectories with t_t in the interval $[(n/2)T, ((n+1)/2)T]$ (T is the optical cycle), we denote them as the n th-return-recollision trajectories [28]. The contributions of different returns to the spectra in Fig. 1(b) are presented in Fig. 2(a)-(c). In the case of the shortest duration of 5 fs (Fig. 2(a)), the 1st-return-recollision trajectories play a dominant role in the plateau, while the contributions of the multiple-return-recollision trajectories can be ignored. When the pulse duration increases to 11

fs (Fig. 2(b)), the contributions of the multiple-return-recollision trajectories increase significantly. The yields of the 2nd and 3rd returns even exceed that of the 1st return. Consequently, the 2nd-return-recollision trajectories become dominant in the low energy part of the plateau while the 3rd-return-recollision trajectories dominate the high energy part. When the pulse duration further increases to 25 fs (Fig. 2(c)), the contributions of the multiple returns continue to increase but much more slightly compared with that from 5 fs to 11 fs. The cutoffs of multiple-return-recollision trajectories, especially the 3rd and 4th return trajectories, also increase with pulse duration, which can be attributed to the variation of the pulse envelope. Since electrons are mostly probably ionized around the maximum of the envelope, the laser field of 5 fs pulse will decrease dramatically when electrons come back to collide with the ions due to steep gradient of the pulse envelope. So the energy cutoffs are much smaller than that in the plane-wave laser field [36, 37]. When the pulse duration increases, the cutoffs increase due to the smaller gradient of pulse envelope. At 25 fs, the cutoff of the 3rd return even becomes equal to the 1st return.

However, according to SFA, trajectories with longer travel time will have smaller probability to collide with the ion due to wave packet spreading. So the multiple-return-recollision trajectories should have smaller contributions to the plateau, which is induced by backscattering, than the 1st-return-recollision trajectories. This can be clearly seen in the results of Yukawa potential in Fig. 2(d), in which the contribution of the 1st return is higher than that of multiple returns. In addition, the cutoff of the 3rd return is significantly lower than the 1st return for Yukawa potential. Therefore, the effect of Coulomb field increases not only the contribution of the 3rd return at the high energy part of the plateau but also the energy cutoff. This is the reason why the plateau exhibits distinct dependence on the pulse duration in Fig. 1.

The dominant contribution of the 3rd return to the spectrum near the cutoff as well as the increase of the cutoff energy can be attributed to modification of the incident (return) electron beam before recollision in the ionic Coulomb potential. The electron beam can be characterized by the temporal evolution of the beam (travel time t_t), the beam energy (recollision energy E_r) and the beam diameter (impact parameter s) as schematically illustrated in Fig. 3(a). In Fig. 3(c)-(d) we present the CTMC calculated 2D distributions of E_r and travel time t_t for Coulomb potential and Yukawa potential, respectively, at pulse duration of 25 fs. The four peaks in each plot correspond directly to the four returns, respectively. The distributions in Figs. 3(c) and (d) are similar except for some details. First, the relative contributions of multiple returns to the 1st return are much smaller in the case of Yukawa potential. Second, in Fig. 3(c) there is a peak on the top of the 3rd return (indicated by dashed line box), while it is absent in the distribution of Yukawa potential in Fig. 3(d). With this peak the recollision en-

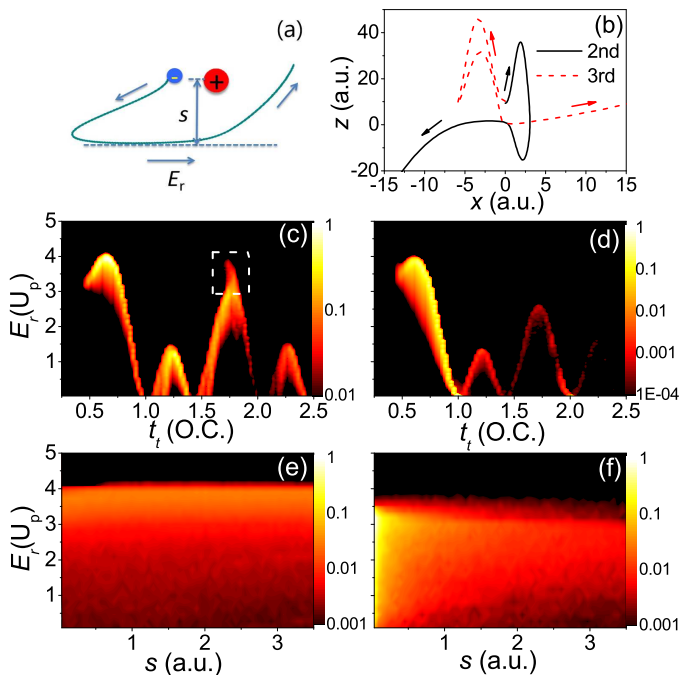


FIG. 3: (Color online) (a) Illustration of the recollision energy E_r and the impact parameter s . (b) Typical 2nd- and 3rd-return-recollision trajectories contributing to the high energy part of the plateau in ATI spectrum. See text for details. (c), (d) 2D distributions of recollision energy E_r and travel time t_t for Coulomb potential and Yukawa potential, respectively. The travel time t_t is defined as the interval between the ionization time and the recollision time. See text for the white dashed line box in (c). (e), (f) 2D distributions of recollision energy E_r and impact parameter s for the 1st- and 3rd-return-recollision trajectories, respectively. The distributions are normalized by dividing the maximum of the 3rd return. The laser parameters are $1.25 \times 10^{14} \text{ W/cm}^2$, 800 nm, and 25 fs.

ergy cutoff of the 3rd return even extends to a value very close to the 1st return as shown in Fig. 3(c). This causes the final energy cutoff of the 3rd return to be identical to the 1st return as shown in Fig. 2(c). After making analysis on the trajectories contributing to the peak on the top of the 3rd return, we find that more than 99% of the trajectories always move on one side of the $z = 0$ plane (laser field is polarized along z axis) before recollision. The typical 3rd return trajectory is shown in Fig. 3(b). For such a trajectory, the Coulomb force on the electron is always in the same direction as the momentum before recollision, which results in an increase of the momentum at recollision. While for the 2nd return and 4th return trajectories, the electrons leave the tunnel exit on one side of the ions but will return to the ions from the other side, so they have to cross the $z = 0$ plane to scatter hardly with the ions to produce high energy electrons. As a result, the Coulomb force will reverse its direction correspondingly, thus the net effect of Coulomb field is negligible. The typical 2nd-return-recollision trajectory is also shown in Fig. 3(b). After making statistics on

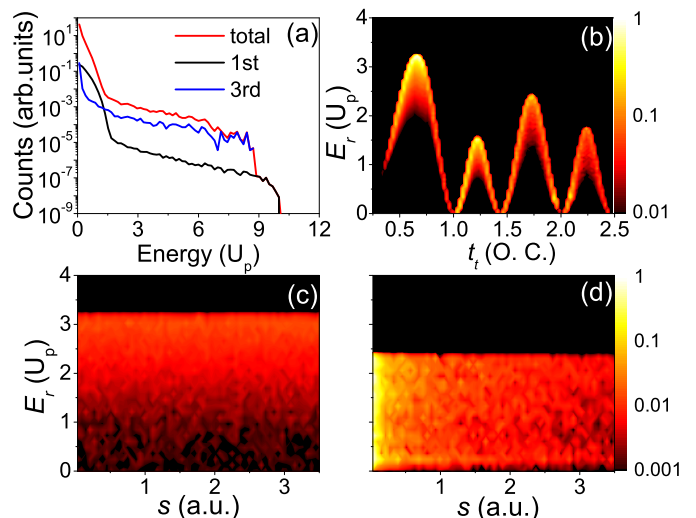


FIG. 4: (Color online) CTMC calculated results for hydrogen-like Ar atoms in laser pulses at peak intensity of $1.25 \times 10^{14} \text{ W/cm}^2$, wavelength of 3100nm and pulse duration of 100 fs. (a) ATI spectra with angle integrated. (b) 2D distribution of recollision energy E_r and travel time t_t . (c), (d) 2D distributions of recollision energy E_r and impact parameter s for the 1st and 3rd returns, respectively. The distributions are normalized by dividing the maximum of the 3rd return.

trajectories contributing to the high energy part of the plateau ($E > 5U_p$) in Fig. 2(c), we find that almost 100% of the 2nd- and 4th-return-recollision trajectories cross the $z = 0$ plane before recollision, while the proportion for the 3rd return is only 50%.

In Figs. 3(e) and 3(f) we plot the 2D distribution for the recollision energy E_r and the impact parameter s for the 1st and the 3rd return, respectively (see supplementary material for details of calculating s). The distributions are normalized to the maximum of the 3rd return to underline the relative contribution between the two returns. The distribution of the 1st return is more concentrated in the high energy region near the maximal return energy but distributes rather uniformly in the impact parameter direction. In contrast, the distribution of the 3rd return is rather uniform in the energy axis but concentrates in the small impact parameter regime. Therefore, the 3rd-return-recollision trajectories are more likely to experience backscattering to produce high energy electrons, and hence its contribution will dominate the ATI spectrum near the cutoff, although the integrated yield of the 1st return in the high recollision energy regime in Fig. 3(c) is considerably larger than that of the 3rd return.

It is noteworthy that laser fields with various wavelengths from infrared to mid-infrared are applied in the LIED scheme to extract time-resolved dynamics of molecules [7–12]. In order to give a more complete assessment of the Coulomb effect in the LIED approach, in Fig. 4 we present the CTMC simulated results for Ar at wavelength of 3100 nm and intensity of $1.25 \times 10^{14} \text{ W/cm}^2$,

which is another kind of typical laser pulse applied in LIED [12]. Overall, the distributions at 3100 nm in Fig. 4 are similar to the results at 800 nm. As shown in Fig. 4(a), the 3rd-return-recollision trajectories dominate the high energy part of the ATI spectrum. In Figs. 4(c) and (d), similar to the case of 800 nm, the 2D distribution of s and E_r for the 1st return distributes uniformly in the impact parameter direction, while the distribution for the 3rd return concentrates in the small impact parameter regime. However, upon a careful inspection, there are some differences between the 800 nm and 3100 nm cases. First, the peak on the top of the 3rd return in Fig. 3(c) disappears in Fig. 4(b). This causes the ATI spectrum cutoff of the 3rd return obviously smaller than the 1st return. As a consequence, a two-step, i.e., two-cutoff structure arises on the spectrum in Fig. 4(a). It should be noted that this two-cutoff structure may not be observed in experiment for two reasons. (i) The signal of the second cutoff is too low for experimental observation; (ii) The realistic cutoff in a quantum system would not be as sharp as in the classical simulations, which makes the two cutoffs hard to be distinguished. Second, the difference between contributions from the 1st return and the 3rd return to the spectrum at 3100 nm is much greater than that at 800 nm, which can be clearly seen by comparing Fig. 4(a) with Fig. 2(c). These differences can be attributed to the weaker effect of Coulomb field at 3100 nm. When wavelength increases, the quiver distance increases quickly but the effective radius of the Coulomb field keeps unchanged, thus the piece of the trajectory affected by the Coulomb field decreases. In addition, the electron momentum also increases and becomes harder to be disturbed by the Coulomb field. Since the peak on the top of the 3rd return in Fig. 3(c) is induced by Coulomb field effect, its absence at 3100 nm is not surprising. The difference of relative contributions between the 1st and 3rd returns can be interpreted with the help of the so-called defocusing effect [38, 39], namely, stronger focusing leads to stronger deflection of the electron at the 1st return, which causes the electron hard to come back to the core at the subsequent returns. Since the Coulomb focus-

ing effect is more prominent for 800 nm, the contribution of the 3rd return is suppressed due to the accompanying enhanced defocusing effect.

Based on the above, we believe that the 3rd-return-recollision trajectories, instead of the 1st ones, should be used for analysis in the LIED scheme. In this case, the imaging results will be affected since the travel time for the 3rd-return-recollision trajectories is about one optical cycle longer than that of the 1st return. Then the extracted result is actually the molecular structure at the time about $7/4 T$ instead of $3/4 T$ after ionization, which is crucial if LIED is applied to investigate the time evolution of the molecular structure after ionization.

In conclusion, we perform a joint investigation on the dependence of ATI spectrum on the pulse duration theoretically and experimentally. The results indicate that the 3rd-return-recollision trajectories dominate the high energy part of the ATI spectrum due to the ionic Coulomb field effect, which invalidates the key assumption of SFA applied in LIED. The incident (return) electron beams associated with different returns show distinct characteristics in the presence of the Coulomb field. Compared with the 1st return, the 3rd return generates an electron beam with a much smaller diameter and a much higher intensity, thus providing more high energy photoelectrons. Moreover, it is found that the Coulomb field will also increase the cutoff energy of the 3rd-return-recollision trajectories, although this effect will become weaker with increasing wavelength. The above Coulomb effect will change the results extracted from the LIED approach and should be taken into account in current imaging schemes based on recollision physics.

This work is supported by the National Key program for S&T Research and Development (No. 2019YFA0307700 and No. 2016YFA0401100), the National Natural Science Foundation of China (Nos. 11504215, 11774387, 11874246, 11834015, 11974383), the Strategic Priority Research Program of the Chinese Academy of Sciences (No. XDB21010400), and the Science and Technology Department of Hubei Province (No. 2019CFA035).

-
- [1] P. B. Corkum, Recollision physics, *Phys. Today* **64**, 36 (2011).
- [2] See a recent *J. Phys. B* issue celebrating the 25th anniversary of recollision physics, for example, D. Faccialá, S. Pabst, B. D. Bruner, A. G. Ciriolo, M. Devetta, M. Negro, P. Prasanna Geetha, A. Pusala, H. Soifer, N. Dudovich, S. Stagira and C. Vozzi, High-order harmonic generation spectroscopy by recolliding electron caustics, *J. Phys. B: At. Mol. Opt. Phys.* **51**, 134002 (2018); M. Krüger, C. Lemell, G. Wachter, J. Burgdörfer and P. Hommelhoff, Attosecond physics phenomena at nanometric tips, *J. Phys. B: At. Mol. Opt. Phys.* **51**, 172001 (2018).
- [3] M. Protopapas, C. H. Keitel and P. L. Knight, Atomic physics with super-high intensity lasers, *Rep. Prog. Phys.* **60**, 389 (1997).
- [4] W. Becker, F. Grasbon, R. Kopold, D. B. Milošević, G. G. Paulus and H. Walther, Above-threshold ionization: from classical features to quantum effects, *Adv. At. Mol. Opt. Phys.* **48**, 35 (2002).
- [5] F. Krausz and M. Ivanov, Attosecond physics, *Rev. Mod. Phys.* **81**, 163 (2009).
- [6] W. Becker, X. Liu, P. J. Ho and J. H. Eberly, Theories of photoelectron correlation in laser-driven multiple atomic ionization, *Rev. Mod. Phys.* **84**, 1011 (2012).
- [7] M. Meckel, D. Comtois, D. Zeidler, A. Staudte, D. Pavičić, H. C. Bandulet, H. Pépin, J. C. Kieffer, R. Dörner, D. M. Villeneuve and P. B. Corkum, Laser-induced electron tunneling and diffraction, *Science* **320**, 1478 (2008).

- [8] C. I. Blaga, J. Xu, A. D. DiChiara, E. Sistrunk, K. Zhang, P. Agostini, T. A. Miller, L. F. DiMauro and C. D. Lin, Imaging ultrafast molecular dynamics with laser-induced electron diffraction, *Nature* **483**, 194 (2012).
- [9] J. Xu, C. I. Blaga, K. Zhang, Y. H. Lai, C. D. Lin, T. A. Miller, P. Agostini and L. F. DiMauro, Diffraction using laser-driven broadband electron wave packets, *Nat. Commun.* **5**, 4635 (2014).
- [10] M. G. Pullen, B. Wolter, A. T. Le, M. Baudisch, M. Sclafani, H. Pires, C. D. Schröter, J. Ullrich, R. Moshhammer, T. Pfeifer, C. D. Lin and J. Biegert, Influence of orbital symmetry on diffraction imaging with rescattering electron wave packets, *Nat. Commun.* **7**, 11922 (2016).
- [11] M. G. Pullen, B. Wolter, A. T. Le, M. Baudisch, M. Hemmer, A. Senftleben, C. D. Schröter, J. Ullrich, R. Moshhammer, C. D. Lin and J. Biegert, Imaging an aligned polyatomic molecule with laser-induced electron diffraction, *Nat. Commun.* **6**, 7262 (2015).
- [12] B. Wolter, M. G. Pullen, A. T. Le, M. Baudisch, K. Doblhoff-Dier, A. Senftleben, M. Hemmer, C. D. Schröter, J. Ullrich, T. Pfeifer, R. Moshhammer, S. Gräfe, O. Vendrell, C. D. Lin and J. Biegert, Ultrafast electron diffraction imaging of bond breaking in di-ionized acetylene, *Science* **354**, 308 (2016).
- [13] H. Niikura, F. Légaré, R. Hasbani, A. D. Bandrauk, M. Y. Ivanov, D. M. Villeneuve and P. B. Corkum, Controlling electron-ion-recollision dynamics with attosecond precision, *Nature* **417**, 917 (2002).
- [14] H. Niikura, F. Légaré, M. Y. Ivanov, D. M. Villeneuve and P. B. Corkum, Probing molecular dynamics with attosecond resolution using correlated wave packet pairs, *Nature* **421**, 826 (2003).
- [15] X. M. Tong, Z. X. Zhao and C. D. Lin, Probing molecular dynamics at attosecond resolution with femtosecond laser pulses, *Phys. Rev. Lett.* **91**, 233203 (2003).
- [16] A. S. Alnaser, X. M. Tong, T. Osipov, S. Voss, C. M. Maharjan, P. Ranitovic, B. Ulrich, B. Shan, Z. Chang, C. D. Lin and C. L. Cocke, Routes to control of H_2 coulomb explosion in few-cycle laser pulses, *Phys. Rev. Lett.* **93**, 183202 (2004).
- [17] J. Itatani, J. Levesque, D. Zeidler, H. Niikura, H. Pépin, J. C. Kieffer, P. B. Corkum and D. M. Villeneuve, Tomographic imaging of molecular orbitals, *Nature* **432**, 867 (2004).
- [18] S. Haessler, J. Caillat, W. Boutu, C. Giovanetti-Teixeira, T. Ruchon, T. Auguste, Z. Diveki, P. Breger, A. Maquet, B. Carré, R. Taïeb and P. Salières, Attosecond imaging of molecular electronic wavepackets, *Nat. phys.* **6**, 200 (2010).
- [19] W. Quan, X. L. Hao, X. Q. Hu, R. P. Sun, Y. L. Wang, Y. J. Chen, S. G. Yu, S. P. Xu, Z. L. Xiao, X. Y. Lai, X. Y. Li, W. Becker, Y. Wu, J. G. Wang, X. J. Liu and J. Chen, Laser-induced inelastic diffraction from strong-field double ionization. *Phys. Rev. Lett.* **119**, 243203 (2017).
- [20] C. I. Blaga, F. Catoire, P. Colosimo, G. G. Paulus, H. G. Muller, P. Agostini and L. F. DiMauro, Strong-field photoionization revisited, *Nat. Phys.* **5**, 335 (2009).
- [21] W. Quan, Z. Lin, M. Wu, H. Kang, H. Liu, J. chen, J. Liu, X. T. He, S. G. Chen, H. Xiong, L. Guo, H. Xu, Y. Fu, Y. Cheng and Z. Z. Xu, Classical aspects in above-threshold ionization with a midinfrared strong laser field, *Phys. Rev. Lett.* **103**, 093001 (2009).
- [22] C. Y. Wu, Y. D. Yang, Y. Q. Liu, Q. H. Gong, M. Wu, X. Liu, X. L. Hao, W. D. Li, X. T. He and J. Chen, Characteristic spectrum of very low-energy photoelectron from above-threshold ionization in the tunneling regime, *Phys. Rev. Lett.* **109**, 043001 (2012).
- [23] W. Quan, X. Hao, Y. J. Chen, S. G. Yu, S. P. Xu, Y. L. Wang, R. P. Sun, X. Y. Lai, C. Y. Wu, Q. H. Gong, X. T. He, X. J. Liu and J. Chen, Long-range coulomb effect in intense laser-driven photoelectron dynamics, *Sci. Rep.* **6**, 27108 (2016).
- [24] D. Shafir, H. Soifer, C. Vozzi, A. S. Johnson, A. Hartung, Z. Dube, D. M. Villeneuve, P. B. Corkum, N. Dudovich and A. Staudte, Trajectory-resolved coulomb focusing in tunnel ionization of atoms with intense, elliptically polarized laser pulses, *Phys. Rev. Lett.* **111**, 023005 (2013).
- [25] M. Li, Y. Q. Liu, H. Liu, Q. C. Ning, L. B. Fu, J. Liu, Y. K. Deng, C. Y. Wu, L. Y. Peng and Q. H. Gong, Subcycle dynamics of coulomb symmetry in strong elliptical laser fields, *Phys. Rev. Lett.* **111**, 023006 (2013).
- [26] T. Brabec, M. Y. Ivanov and P. B. Corkum, Coulomb focusing in intense field atomic processes, *Phys. Rev. A* **54**, R2551 (1996).
- [27] G. L. Yudin and M. Y. Ivanov, Physics of correlated double ionization of atoms in intense laser fields: Quasistatic tunneling limit, *Phys. Rev. A* **63**, 033404 (2001).
- [28] X. L. Hao, W. D. Li, J. Liu and J. Chen, Effect of the electron initial longitudinal velocity on the nonsequential double-ionization process, *Phys. Rev. A* **83**, 053422 (2011).
- [29] X. Y. Jia, X. L. Hao, D. H. Fan, W. D. Li and J. Chen, S-matrix and semiclassical study of electron-electron correlation in strong-field nonsequential double ionization of Ne, *Phys. Rev. A* **88**, 033402 (2013).
- [30] B. Hu, J. Liu and S. G. Chen, Plateau in above-threshold-ionization spectra and chaotic behavior in rescattering processes, *Phys. Lett. A* **236**, 533 (1997).
- [31] J. Chen, J. Liu and S. G. Chen, Rescattering effect on phase-dependent ionization of atoms in two-color intense fields, *Phys. Rev. A* **61**, 033402 (2000).
- [32] D. Bauer and P. Koval, QPROP: A Schrödinger-solver for intense laser-atom interaction, *Comput. Phys. Commun.* **174**, 396 (2006); see also [<http://www.qprop.de>].
- [33] W. Quan, X. Y. Lai, Y. J. Chen, C. L. Wang, Z. L. Hu, X. J. Liu, X. L. Hao, J. Chen, E. Hasović, M. Busuladžić, W. Becker and D. B. Milošević, Resonancelike enhancement in high-order above-threshold ionization of molecules, *Phys. Rev. A* **88**, 021401(R) (2013).
- [34] X. Y. Lai, W. Quan, S. G. Yu, Y. Y. Huang and X. J. Liu, Suppression in high-order above-threshold ionization: destructive interference from quantum orbits, *J. Phys. B* **51**, 104003 (2018).
- [35] Calculation of CTMC shows that the spectrum nearly has no change when pulse duration further increases to 50 fs. The spectrum of 50 fs is presented in the supplementary material.
- [36] G. G. Paulus, W. Becker, W. Nicklich and H. Walther, Rescattering effects in above-threshold ionization: a classical model, *J. Phys. B: At. Mol. Opt. Phys.* **27**, L703 (1994).
- [37] X. H. Tu, X. L. Hao, W. D. Li, S. L. Hu and J. Chen, Nonadiabatic effect on the rescattering trajectories of electrons in strong laser field ionization process, *Chin. Phys. Lett.* **33**, 093201 (2016).
- [38] S. A. Kelvich, W. Becker and S. P. Goreslavski, Coulomb focusing and defocusing in above-threshold ionization

- spectra produced by strong mid-IR laser pulses, Phys. Rev. A **93**, 033411 (2016).
- [39] Y. L. Wang, S. P. Xu, Y. J. Chen, H. P. Kang, X. Y. Lai, W. Quan, X. J. Liu, X. L. Hao, W. D. Li, S. L. Hu, J. Chen, W. Becker, W. Chu, J. P. Yao, B. Zeng, Y. Cheng and Z. Z. Xu, Wavelength scaling of atomic nonsequential double ionization in intense laser fields, Phys. Rev. A **95**, 063415 (2017).